

Mechanistic Studies of Single-Step Styrene Production Using a Rhodium(I) Catalyst

Benjamin A. Vaughan,[†] Sarah K. Khani,[‡] J. Brannon Gary,[‡] James D. Kammert,[#] Michael S. Webster-Gardiner,[†] Bradley A. McKeown,[†] Robert J. Davis,[#] Thomas R. Cundari,^{*,‡} and T. Brent Gunnoe^{*,†}

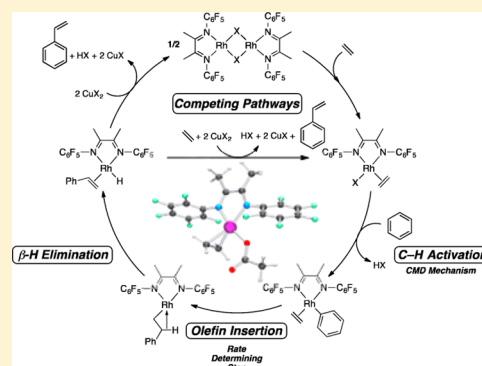
[†]Department of Chemistry, University of Virginia, Charlottesville, Virginia 22904, United States

[‡]Center for Advanced Scientific Computing and Modeling, Department of Chemistry, University of North Texas, Denton, Texas 76203, United States

[#]Department of Chemical Engineering, University of Virginia, Charlottesville, Virginia 22904, United States

S Supporting Information

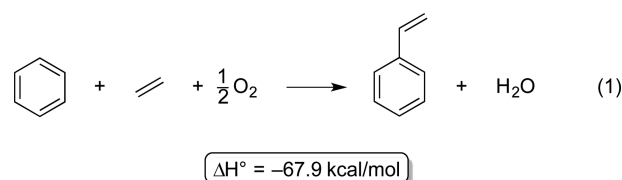
ABSTRACT: The direct and single-step conversion of benzene, ethylene, and a Cu(II) oxidant to styrene using the Rh(I) catalyst (^{Fl}DAB)Rh(TFA)(η^2 -C₂H₄) [^{Fl}DAB = *N,N'*-bis(pentafluorophenyl)-2,3-dimethyl-1,4-diaza-1,3-butadiene; TFA = trifluoroacetate] has been reported to give quantitative yields (with Cu(II) as the limiting reagent) and selectivity combined with turnover numbers >800. This report details mechanistic studies of this catalytic process using a combined experimental and computational approach. Examining catalysis with the complex (^{Fl}DAB)Rh(OAc)(η^2 -C₂H₄) shows that the reaction rate has a dependence on catalyst concentration between first- and half-order that varies with both temperature and ethylene concentration, a first-order dependence on ethylene concentration with saturation at higher concentrations of ethylene, and a zero-order dependence on the concentration of Cu(II) oxidant. The kinetic isotope effect was found to vary linearly with the order in (^{Fl}DAB)Rh(OAc)(η^2 -C₂H₄), exhibiting no KIE when [Rh] was in the half-order regime, and a k_H/k_D value of 6.7(6) when [Rh] was in the first-order regime. From these combined experimental and computational studies, competing pathways, which involve all monomeric Rh intermediates and a binuclear Rh intermediate in the other case, are proposed.



INTRODUCTION

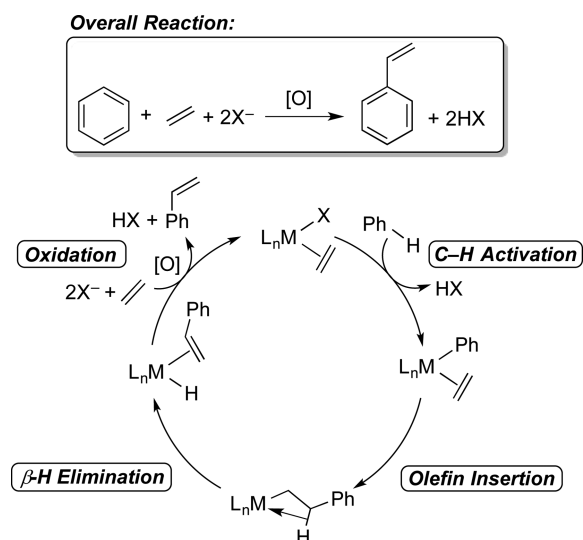
Styrene is produced on a scale of ~18.5 million tons annually for use in plastics, elastomers, and fine chemicals.^{1–5} Industrial synthesis of styrene often involves an acid-catalyzed (i.e., Friedel–Crafts or zeolite catalysis) arene alkylation to form ethylbenzene, trans-alkylation to optimize yield, and ethylbenzene dehydrogenation.^{1–10} Although this method has been employed by industry for many years, there are some disadvantages.² Dehydrogenative addition of an arene C–H bond across an olefin C=C bond (i.e., oxidative arene vinylation) provides a potential route to directly synthesize vinyl arenes from arenes, olefins, and oxidants. For styrene production, one possible route involves metal-mediated activation of the C–H bond of benzene to yield a M–Ph bond, ethylene insertion into the resulting M–Ph bond to produce a M–CH₂CH₂Ph complex, and β -hydride elimination from the resulting M–CH₂CH₂Ph complex to give coordinated styrene and a M–H bond (Scheme 1). Subsequent styrene dissociation (regardless of mechanism) and reaction with oxidant can regenerate the active catalyst, and if the oxidant is oxygen (either used *in situ* or used to recycle an *in situ* oxidant),

the net reaction is the thermodynamically favorable conversion of benzene, ethylene, and oxygen to styrene and water (eq 1).¹¹



While catalysts have been developed for the addition of unactivated arene C–H bonds (i.e., non-heterofunctionalized arenes such as benzene, toluene, naphthalene, etc.) across olefin C=C bonds (i.e., catalytic olefin hydroarylation) to afford alkyl arenes,^{12–24} few examples of transition metal catalysts for oxidative arene vinylation using unactivated substrates have been reported.^{25–30} Of the reported catalysts, to our knowledge, all suffer from low selectivity and/or low yield/catalytic turnovers. For example, Hong and co-workers reported a

Received: October 11, 2016

Scheme 1. Catalytic Cycle for Transition-Metal-Catalyzed Styrene Production from Benzene, Ethylene, and Oxidant^a

^a[O] denotes 1 equiv of a two-electron oxidant or 2 equiv of a one-electron oxidant.

Rh₄(CO)₁₂ catalyst that affords 472 turnovers (TO) of styrene; however, 809 TO of a byproduct (3-pentanone) are also produced.²⁵ Another example is the work of Sanford and co-workers, who have reported that (3,5-dichloropyridyl)Pd(OAc)₂ catalyzes styrene production with 100% selectivity, but the overall turnover number is low (6.6 TO, 33% overall yield) and the reaction incorporates the expensive oxidant PhCO₃^tBu that cannot be readily regenerated from air or dioxygen.²⁹ Germane here, Periana and co-workers have disclosed styrene production using Rh(III) complexes.²⁶

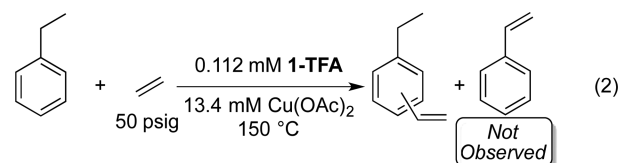
In an initial communication, we reported that the Rh(I) complex (^{Fl}DAB)Rh(TFA)(η^2 -C₂H₄) (**1-TFA**) [^{Fl}DAB = *N,N'*-bis(pentafluorophenyl)-2,3-dimethyl-1,4-diaza-1,3-butadiene; TFA = trifluoroacetate] effectively catalyzes the conversion of benzene and ethylene to styrene in the presence of Cu(II) oxidants.³¹ This catalyst affords quantitative yields of styrene (relative to the Cu(II) limiting reagent) with quantitative selectivity and gives turnover numbers (TON) > 800. Catalysis with **1-TFA** is also one of the longest-lived catalytic processes for styrene production using a molecular catalyst, showing activity for up to 96 h with apparent turnover frequencies (TOF) on the order of 10⁻³ s⁻¹. Herein, we report a mechanistic study of catalysis with **1-TFA**.

RESULTS AND DISCUSSION

Initial studies of arene C–H activation in acidic media by the cyclooctene variant of **1-TFA** revealed fast rates of benzene C–H activation.³² Since C–H activation is a key step in the mechanism for oxidative arene vinylation, these results indicated that **1-TFA** might be an effective catalyst for vinyl arene production. Upon reaction of benzene with ethylene in the presence of **1-TFA** and Cu(II) oxidant, styrene is formed with high selectivity. As disclosed in a preliminary communication,³¹ this catalysis was examined over a range of conditions, and optimal yields and reaction rates were achieved at 150 °C using Cu(OAc)₂ as the oxidant.

Since our general mechanistic hypothesis for styrene production (Scheme 1) involves the direct conversion of

benzene and ethylene to styrene without the intermediacy of ethylbenzene, we first sought to confirm that ethylbenzene is not converted to styrene under catalytic conditions using **1-TFA** (eq 2). Heating a solution of **1-TFA** and Cu(OAc)₂ in



ethylbenzene under 50 psig of ethylene showed no formation of styrene after 8 h. Isomers of ethyl-vinylbenzene were detected, but not quantified, by GC/MS.

Apparent Induction Period. Under some conditions, monitoring the conversion of benzene, ethylene, and Cu(OAc)₂ to styrene and CuOAc catalyzed by **1-TFA** reveals an apparent induction period (see Figure 1, for example). We investigated

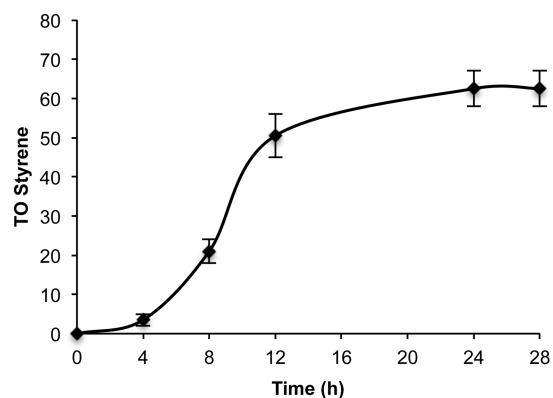


Figure 1. TO vs time plot for catalysis with **1-TFA**. Reaction conditions: 0.112 mM **1-TFA**, 20 mL C₆H₆, 25 psig ethylene, 13.4 mM Cu(OAc)₂ (120 equiv relative to **1-TFA**), 150 °C. Each data point is the average of two independent catalytic reactions, each analyzed in duplicate by GC/FID. Error bars represent the standard deviation of all four values.

two possible rationalizations for the observed change in rate of catalysis: (1) the active catalyst is formed by decomposition of **1-TFA** to insoluble Rh nanoparticles that catalyze the reaction,³³ and (2) during the apparent induction period, **1-TFA** converts to (^{Fl}DAB)Rh(OAc)(η^2 -C₂H₄) (**1-OAc**), and **1-OAc** catalyzes the reaction at a faster rate than **1-TFA**.

Testing for Nanoparticle Formation. A number of tests for the formation of nanoparticles from the decomposition of homogeneous complexes are known;³⁴ however, some of these methods are unsuitable for use with rhodium (e.g., the mercury drop test, which is unsuitable since Rh does not amalgamate well).³⁴ One method for the detection of nanoparticles is transmission electron microscopy (TEM). While it has been argued that TEM might not provide useful information regarding the formation of nanoparticles due to its inherent inability to detect particles below 1 nm in size,³⁴ when coupled with energy-dispersive X-ray spectroscopy (EDS), which provides information about elemental composition of samples, this method can provide evidence for or against the formation of nanoparticles.

We performed TEM/EDS experiments on samples of reaction mixtures from catalysis with **1-TFA**. Catalytic reactions with **1-TFA** and Cu(OAc)₂ were allowed to reach completion,

after which samples were deposited on a grid, allowed to evaporate, and analyzed by TEM and EDS. While many of the sample regions chosen for TEM imaging appeared to contain nanoparticles (Figure 2A), EDS results show that these regions do not contain Rh. Interestingly, some of the regions that

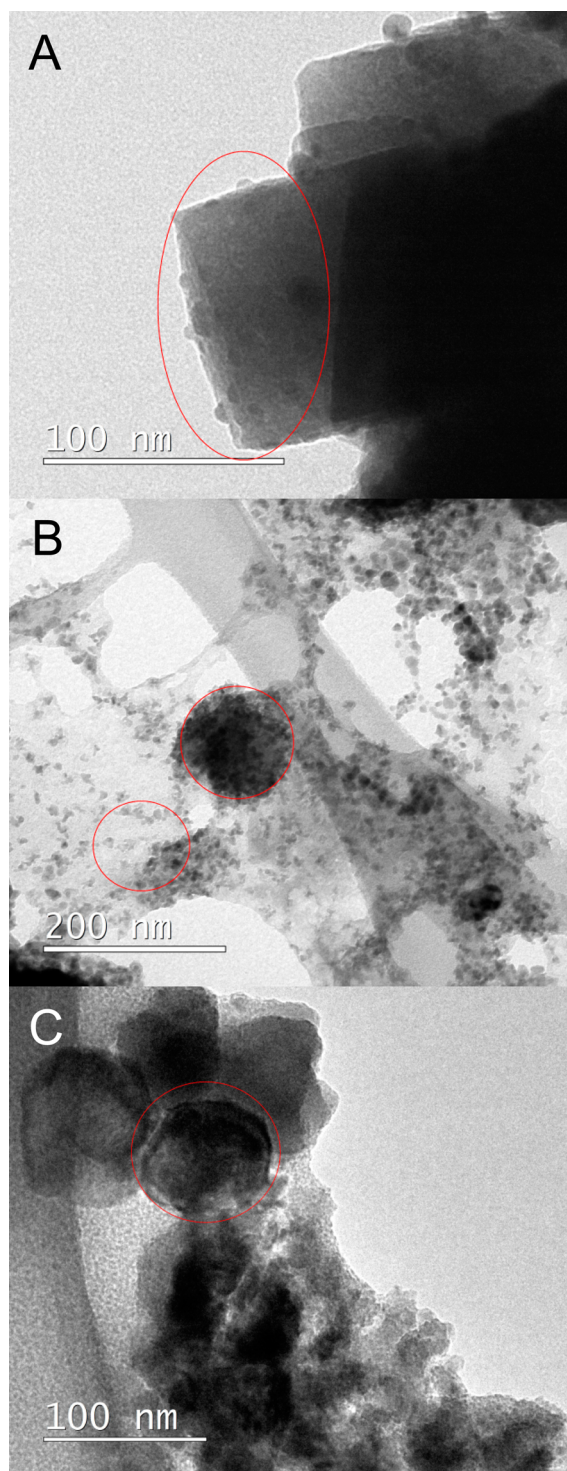


Figure 2. TEM images of reaction mixtures from catalysis with 1-TFA. EDS was performed on circled areas. (A) Unwashed sample, region with nanoparticle-like structures. (B) Unwashed sample, amorphous region. (C) Solid from catalytic reaction deposited after washing with dioxane. Reaction conditions for catalysis: 0.112 mM 1-TFA, 20 mL C_6H_6 , 50 psig ethylene, 13.4 mM $Cu(OAc)_2$, 150 °C, 12 h.

appeared to be amorphous (Figure 2B) showed significant concentrations of Rh by EDS. We hypothesized that this was likely a result of remaining molecular Rh complex on the sample grid. To test this hypothesis, samples of neat reaction mixture were decanted to leave only solid (mostly Cu) and remove any soluble materials. The solid was subsequently sonicated in dioxane (in which 1-TFA is soluble), decanted, and the remaining solid was deposited on the grid. Results from EDS of these washed samples showed no Rh present (Figure 2C). As an additional control, the solid material isolated by filtration was subjected to catalytic conditions, and styrene production was not observed after 12 h of heating.

In addition to the TEM/EDS analysis, we performed the Maitlis filtration test (Figure 3).³⁵ Reactions with 1-TFA and

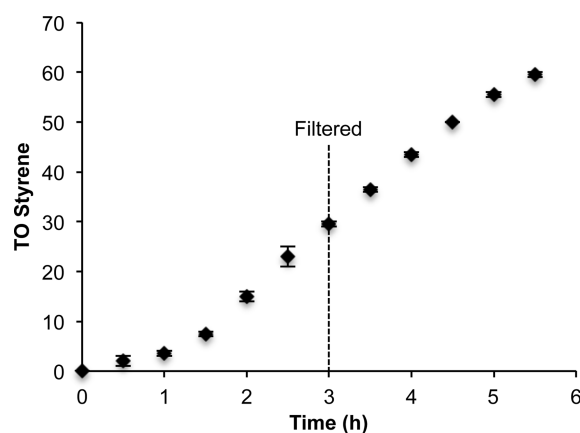


Figure 3. TO vs time plot with the reaction solution filtered at 3 h. Reaction conditions: 0.112 mM 1-TFA, 20 mL C_6H_6 , 50 psig ethylene, 13.4 mM $Cu(OPiv)_2$ (120 equiv relative to 1-TFA), 150 °C. Each data point is the average of two independent catalytic reactions, each analyzed in duplicate by GC/FID. Error bars represent the standard deviation of all four values.

$Cu(OPiv)_2$ (OPiv = pivalate) were sampled every 30 mins until 3 h, at which time the reaction mixture was filtered through Celite and the reactors were recharged with the filtrate and heated to 150 °C (n.b.: $Cu(OPiv)_2$ was used due to its solubility in benzene). The filtration should remove insoluble Rh materials, and a second induction period would be expected if insoluble materials were serving as the active catalyst. The results from both the TEM and Maitlis test experiments suggest that insoluble nanoparticles are not serving as the catalyst, and therefore, that formation of insoluble Rh nanoparticles is likely not the reason for the apparent induction period.

Comparison of Catalysis with 1-TFA and 1-OAc.

Operating under the assumption that catalysis proceeds by a pathway similar to that shown in Scheme 1, we hypothesized that 1-TFA converts to 1-OAc *in situ* (e.g., after completing one catalytic loop and releasing HTFA). To test this hypothesis, 1-OAc was independently synthesized and tested for catalytic activity. Under identical conditions as catalysis with 1-TFA, the reaction with 1-OAc using $Cu(OPiv)_2$ shows no apparent induction period. $Cu(OPiv)_2$ was used in place of $Cu(OAc)_2$ due to the enhanced solubility of $Cu(OPiv)_2$ and the likely similar reactivity of Rh-OAc and Rh-OPiv intermediates. This result is consistent with 1-OAc serving as a more active catalyst compared to 1-TFA. We compared the rate of catalysis of 1-OAc to 1-TFA after the apparent induction period using a plot of [styrene] vs time in which data for 1-OAc are time-shifted (*t*

= 0.5 h shifted to $t = 1.5$ h) and overlaid with data from reactions using **1-TFA** as the catalyst precursor (Figure 4). The

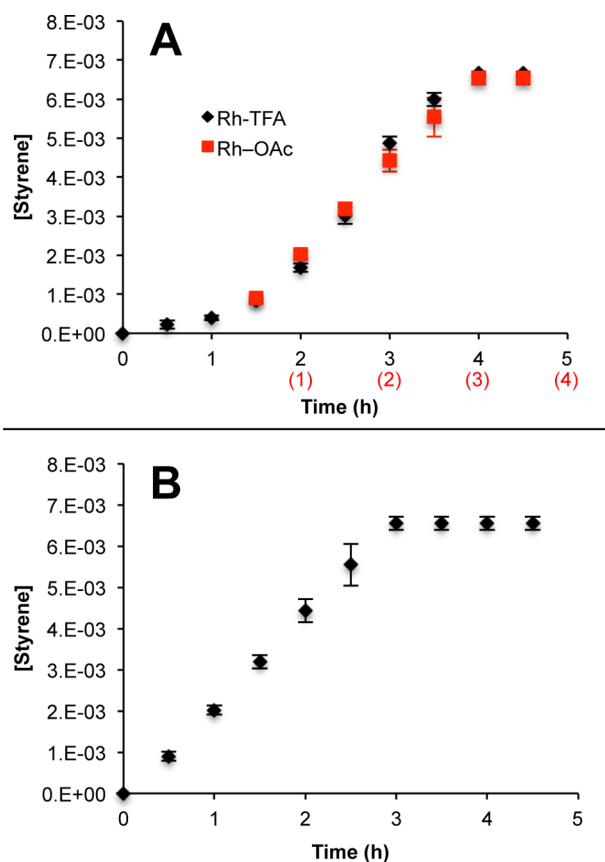


Figure 4. (A) [Styrene] vs time plot for catalysis with **1-TFA** and **1-OAc** using $\text{Cu}(\text{OPiv})_2$ as the oxidant. Reaction conditions: 0.112 mM **1-TFA** or **1-OAc**, 20 mL C_6H_6 , 13.4 mM $\text{Cu}(\text{OPiv})_2$ (120 equiv relative to **1-TFA** or **1-OAc**), 50 psig C_2H_4 , 150 °C. Data for **1-OAc** are offset from $t = 0.5$ h to $t = 1.5$ h to overlap with data from **1-TFA**, and non-offset times are labeled in red. Each data point is the average of two independent catalytic reactions, each analyzed in duplicate by GC/FID. Error bars represent the standard deviation of all four values. (B) [Styrene] vs time plot for catalysis with **1-OAc** from panel A without time offset, which is consistent with no induction period.

overlap of the plots shows nearly identical [styrene] versus time profiles for catalysis following the apparent induction period for **1-TFA**, which supports the hypothesis that **1-TFA** is converting to **1-OAc** *in situ*.

We performed catalytic experiments with **1-TFA** using both $\text{Cu}(\text{TFA})_2$ and $\text{Cu}(\text{OAc})_2$ as oxidants. Plots of TO vs time for these reactions are shown in Figure 5. For catalysis using $\text{Cu}(\text{TFA})_2$, a consistently slower rate is observed. For the reaction with $\text{Cu}(\text{OAc})_2$, the rate of catalysis gradually increases, which is consistent with conversion of **1-TFA** to **1-OAc**. For reactions using **1-TFA** and $\text{Cu}(\text{TFA})_2$, we do not observe induction periods.

Computational Studies: Overview. To gain insight into the difference in rate of catalysis for **1-TFA** compared to **1-OAc**, we performed a computational study (B3LYP) of the fundamental steps involved in the proposed catalytic cycle (Scheme 2). The catalytic cycle we modeled involves (a) benzene coordination to $(^{\text{Fl}}\text{DAB})\text{Rh}(\eta^2\text{-C}_2\text{H}_4)(\text{X})$ by net ligand substitution with ethylene and subsequent benzene C–H activation, (b) ethylene coordination and insertion into the

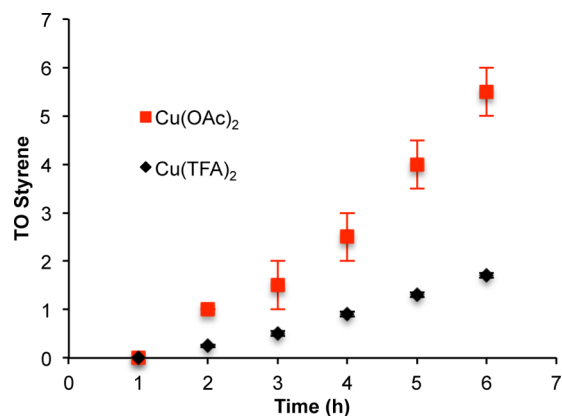
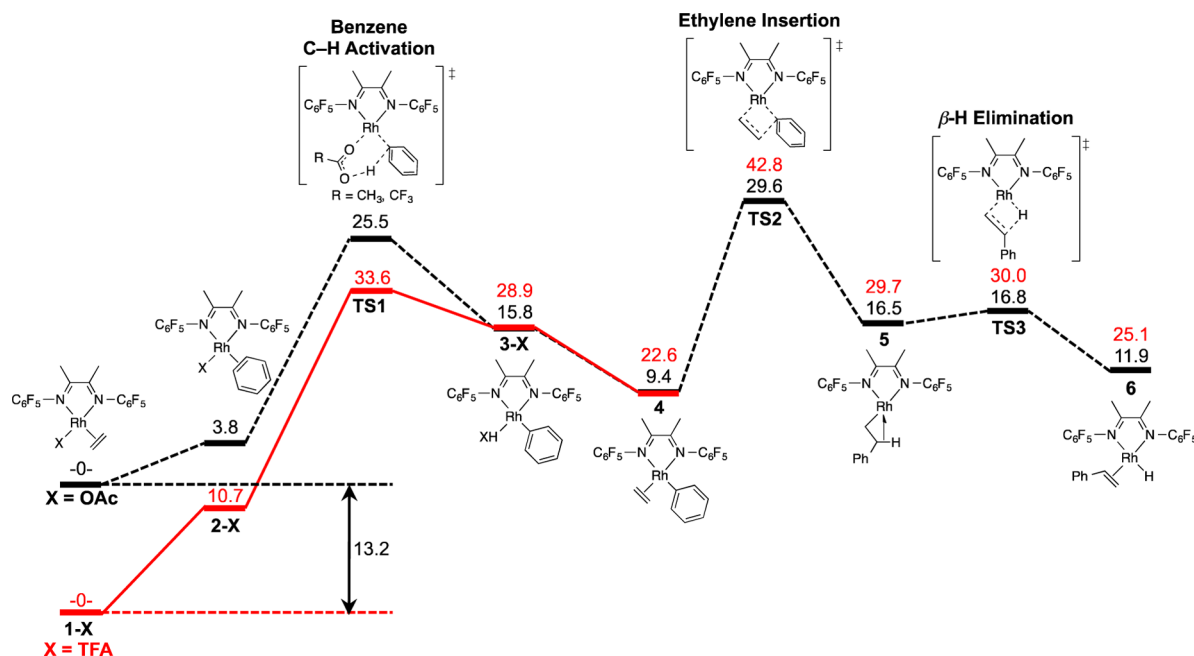


Figure 5. TO vs time plot for catalysis with **1-TFA** using $\text{Cu}(\text{OAc})_2$ or $\text{Cu}(\text{TFA})_2$ as the oxidant. Reaction conditions: 0.112 mM **1-TFA**, 20 mL C_6H_6 , 13.4 mM CuX_2 (120 equiv relative to **1-TFA**), 25 psig C_2H_4 , 150 °C. Each data point is the average of two independent catalytic reactions, each analyzed in duplicate by GC/FID. Error bars represent the standard deviation of all four values.

Rh–Ph bond, (c) β -hydride elimination from the Rh- $\text{CH}_2\text{CH}_2\text{Ph}$ intermediate, and (d) styrene dissociation. To display the results of these calculations in an easily viewed comparison, in Scheme 2 we set the free energy of each of the complexes **1-OAc** or **1-TFA** to zero. Our calculations also included the energetics of conversion of **1-TFA** and **1-OAc** to the dimers $[(^{\text{Fl}}\text{DAB})\text{Rh}(\mu\text{-X})]_2$ (X = OAc or TFA; **1D-OAc** or **1D-TFA**, respectively). Using the B3LYP functional, the dimers were calculated to be more stable than the monomeric species **1-TFA** and **1-OAc** by 11.2 and 6.3 kcal/mol, respectively. In contrast to these calculations, experimental results indicate that the monomeric complexes are more stable than the dimers. For example, a C_6D_6 solution of independently synthesized **1D-TFA** completely converts to **1-TFA** in the presence of ethylene at room temperature in <1 min. As a result of the discrepancy between experimental and computational results, the conversions of monomer to dimer were computationally modeled using the M06 functional, which gave ΔG values (dimer to monomer) of -1.8 and 1.5 kcal/mol for **1-TFA** and **1-OAc** at 423 K, respectively, which are more in line with experimental observations. The M06 functional is known to provide better estimates of van der Waals interactions, which we believe gives a more accurate modeling of the energetics for monomer/dimer interconversion. However, to assess catalysis based on monomeric catalysts, we retained the B3LYP data. The calculations predict $\Delta G^\ddagger = 29.6$ kcal/mol using **1-OAc** and $\Delta G^\ddagger = 42.8$ kcal/mol using **1-TFA**. These barriers are consistent with experimental rates. Using the Eyring equation, k_{obs} values (for details on k_{obs} calculations, *vide infra*) from reactions using **1-TFA** with $\text{Cu}(\text{TFA})_2$ as the oxidant (which results in the Rh-TFA moiety being retained throughout catalysis) and **1-OAc** with $\text{Cu}(\text{OAc})_2$ as the oxidant (which results in the Rh-OAc moiety being retained throughout catalysis) give ΔG^\ddagger values which are in general agreement with ΔG^\ddagger values from computations (for Rh-TFA, 42.8 kcal/mol; for Rh-OAc, 29.6 kcal/mol).

From the complexes **1-OAc** and **1-TFA**, multiple possible pathways for benzene C–H activation were calculated. The lowest energy pathway for catalysis by both **1-OAc** and **1-TFA** involves initial displacement of ethylene to afford the corresponding η^2 -benzene complexes $(^{\text{Fl}}\text{DAB})\text{Rh}(\text{OAc})(\eta^2\text{-C}_6\text{H}_6)$ [**2-OAc**] and $(^{\text{Fl}}\text{DAB})\text{Rh}(\text{TFA})(\eta^2\text{-C}_6\text{H}_6)$ [**2-TFA**]

Scheme 2. Calculated Gibbs Free Energies [B3LYP/LANL2DZ+6-311++G(d,p) in kcal/mol] Including Solvent (SMD-benzene) and Dispersion Corrections for the Lowest Energy Calculated Pathway for Styrene Production Using Complexes 1-OAc (Shown in Black) and 1-TFA (Shown in Red) at 423.15 K^a



^aThe calculated energies for each reaction are relative to the energy of 1-X (X = OAc or TFA), which is set to zero energy for each reaction. Stationary points without TFA or OAc are degenerate.

with energies of 3.8 and 10.7 kcal/mol relative to 1-OAc and 1-TFA, respectively. It is interesting to note that ethylene/benzene exchange is ~ 7 kcal/mol less favorable for 1-TFA than for 1-OAc, accounting for $\sim 50\%$ of the calculated overall $\Delta\Delta G^\ddagger$ of 13.2 kcal/mol for the catalytic process.

Following the formation of a benzene adduct, the lowest energy C–H activation pathway for both complexes was found to involve concerted metalation–deprotonation (CMD) of benzene using an acetate ligand,^{36–42} with activation barriers of 21.7 kcal/mol for the Rh-OAc complex and 22.9 kcal/mol for the Rh-TFA complex relative to 2-OAc and 2-TFA, respectively. After benzene C–H activation, the coordinated HX is displaced by ethylene to generate $(^{\text{Fl}}\text{DAB})\text{Rh}(\text{Ph})(\eta^2\text{-C}_2\text{H}_4)$ (4). Comparing the optimized transition-state geometries for CMD of benzene from 2-OAc and 2-TFA (Figure 6), it can be observed that the Rh–C and C–O bond lengths (2.19 and 1.25 Å, respectively, for the Rh-TFA transition state) elongate by 0.02 Å for the Rh-OAc transition state. Conversely, the Rh–O bond length shrinks by 0.02 Å. More noticeable is the change in the C–H bond distance in the Rh-TFA transition state, which is 0.06 Å longer than the corresponding bond in the Rh-OAc transition state; the O–H bond in the Rh-OAc transition state is elongated by 0.06 Å versus the same bond in the Rh-TFA transition state. Hence, the transition state for the Rh-TFA complex appears to be later than the corresponding transition state for Rh-OAc, which is consistent with the Hammond postulate, as the ΔH for benzene C–H activation by 2-TFA is calculated to be more endothermic ($\Delta H = 17.3$ kcal/mol) and endergonic ($\Delta G = 18.2$ kcal/mol) than that of 2-OAc ($\Delta H = 12.9$ kcal/mol, $\Delta G = 12.0$ kcal/mol).

Previous studies of ethylene insertion into Pt(II) hydrocarbyl and aryl bonds demonstrate the viability of such reactions for cationic complexes, but the results suggest that the activation barrier for olefin insertion might be higher for overall charge-

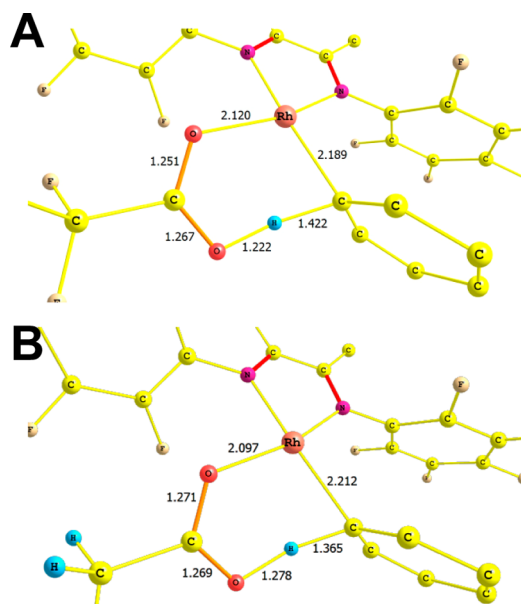
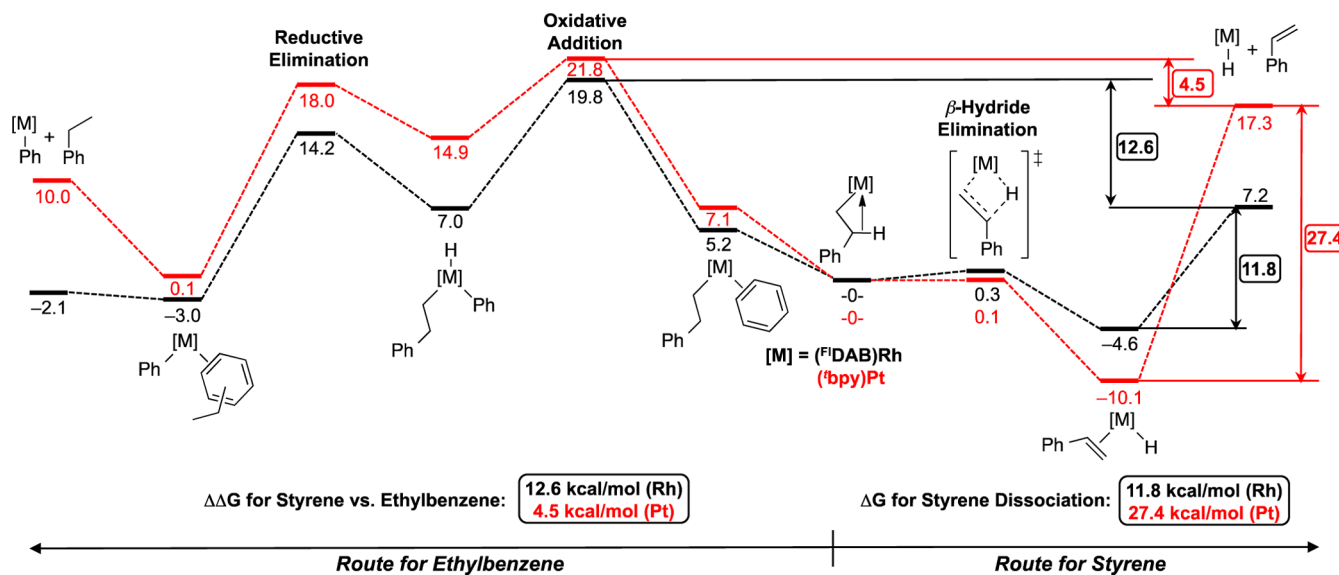


Figure 6. Optimized calculated geometries for the transition states for benzene C–H activation by (A) $(^{\text{Fl}}\text{DAB})\text{Rh}(\eta^2\text{-C}_6\text{H}_6)(\text{TFA})$ (2-TFA), and (B) $(^{\text{Fl}}\text{DAB})\text{Rh}(\eta^2\text{-C}_6\text{H}_6)(\text{OAc})$ (2-OAc). Bond lengths in Å.

neutral complexes than for cationic complexes.²² Thus, we anticipated that activation barriers for ethylene insertion into Rh–Ph bonds of charge-neutral Rh(I) complexes might be higher than those of related Pt(II) complexes. Previously, we have shown that the conversion of $[(^{\text{t}}\text{bpy})\text{Pt}(\text{Ph})(\text{THF})]^+$ ($^{\text{t}}\text{bpy} = 4,4'$ -di-*tert*-butyl-2,2'-bipyridyl) and ethylene to $[(^{\text{t}}\text{bpy})\text{Pt}(\text{CH}_2\text{CH}_2\text{Ph})(\eta^2\text{-C}_2\text{H}_4)]^+$ at 23 °C occurs with an experimentally determined ΔG^\ddagger of 21.0(1) kcal/mol.¹⁷ This

Scheme 3. Comparison of Calculated Free Energies (in kcal/mol) for β -Hydride Elimination To Form Styrene and Benzene C–H Activation To Form Ethylbenzene from $(^{\text{Fl}}\text{DAB})\text{Rh}(\text{CH}_2\text{CH}_2\text{Ph})$ (Shown in Black) and $(^{\text{t}}\text{bpy})\text{Pt}(\text{CH}_2\text{CH}_2\text{Ph})$ (Shown in Red), with the Important Energy Differences between the Two Pathways Highlighted



activation energy is similar to the reported ΔG^\ddagger of 19.2 kcal/mol for ethylene insertion into a Pt(II)–hydride bond.⁴³ Through the use of a diimine ligand with electron-withdrawing perfluorophenyl groups (i.e., $^{\text{Fl}}\text{DAB}$) we sought to generate a Rh center with similar properties to cationic Pt(II) such as $[(^{\text{X}}\text{bpy})\text{Pt}(\text{Ph})(\text{THF})]^+$ ($^{\text{X}}\text{bpy}$ = 4,4'-X-2,2'-bipyridyl).^{14,17,19–22} Insertion of ethylene into the Rh–Ph bond of $(^{\text{Fl}}\text{DAB})\text{Rh}(\text{Ph})(\eta^2\text{-C}_2\text{H}_4)$ (**4**) is calculated to have a free energy of activation of 20.2 kcal/mol from complex **4**, which is commensurate with the cationic Pt(II) complex $(^{\text{t}}\text{bpy})\text{Pt}(\text{Ph})(\eta^2\text{-C}_2\text{H}_4)$, for which the free energy of activation for ethylene insertion into the Pt–Ph bond was calculated to be 21.5 kcal/mol. (n.b.: to provide an accurate comparison, the energy values for Pt complexes¹⁷ have been recalculated using the same computational parameters as have been used for the Rh complexes presented herein).

For catalysis with **1-OAc**, the $\Delta\Delta G^\ddagger$ between C–H activation and olefin insertion is 4.1 kcal/mol, suggesting that ethylene insertion is the rate-determining step. For catalysis with **1-TFA**, the $\Delta\Delta G^\ddagger$ for the same two steps is 9.2 kcal/mol, and also predicts that ethylene insertion is the rate-determining step. This is in contrast to Pt(II)- and Ru(II)-based catalysts for ethylbenzene formation for which C–H activation is calculated to be rate-determining.^{13,17} We note that some calculations for the Ru(II) catalyst indicated ethylene insertion as the rate-determining step.⁴⁴ The calculations are consistent with a kinetic advantage for **1-OAc** over **1-TFA**. The calculated $\Delta\Delta G^\ddagger$ for catalysis using **1-OAc** vs **1-TFA** is 13.2 kcal/mol, and computational modeling suggests that the difference in ground-state energies of **1-OAc** and **1-TFA** greatly influences the difference in rate of catalysis. The penultimate step in the pathway for styrene production is β -hydride elimination, which was calculated to have an activation barrier of only 0.3 kcal/mol relative to $(^{\text{Fl}}\text{DAB})\text{Rh}(\text{CH}_2\text{CH}_2\text{Ph})$ (**5**).

The calculations predict different rate-determining steps for ethylene hydrophenylation by $[(^{\text{t}}\text{bpy})\text{Pt}(\text{Ph})(\text{THF})]^+$ and oxidative hydrophenylation of ethylene by **1-TFA/1-OAc**. For the Pt catalyst, the transition state for benzene C–H activation is calculated to be the highest energy species, while

the transition state for ethylene insertion is the calculated highest energy species for the Rh catalysis. Notably, for the Pt catalysis an *inverse* dependence on ethylene concentration was experimentally demonstrated, while for the Rh catalysis a first-order dependence is observed (*vide infra*).¹⁷

Computational Studies: Selectivity for Styrene. A challenge for oxidative arene vinylation has been achieving selectivity for the vinyl arene product. In fact, $[(^{\text{t}}\text{bpy})\text{Pt}(\text{THF})(\text{Ph})]^+$ has been reported to selectively yield ethylbenzene, even in the presence of oxidants including various Cu(II) salts (unpublished results).^{17,20} As noted below, modification of the donor ability of the 2,2'-bipyridyl ligand coordinated to Pt(II) can result in the production of styrene, and in one case a few turnovers are observed with ethylene as the oxidant.²⁰ From a $\text{M-CH}_2\text{CH}_2\text{Ph}$ intermediate, ethylbenzene is formed from benzene C–H activation, whereas styrene is formed from β -hydride elimination and net styrene dissociation. In order to understand why the $[(^{\text{t}}\text{bpy})\text{Pt}(\text{Ph})]^+$ catalyst intermediate is selective for ethylbenzene production while the $(^{\text{Fl}}\text{DAB})\text{Rh}(\text{Ph})$ intermediate is selective for styrene production, we modeled the likely reaction steps for each product, which are shown in Scheme 3. The two pathways to form either styrene or ethylbenzene diverge from the $\text{M-CH}_2\text{CH}_2\text{Ph}$ intermediate. In the pathway to form styrene, β -hydride elimination occurs to give a $\text{M}(\text{H})(\eta^2\text{-styrene})$ intermediate that subsequently liberates styrene. In the pathway to form ethylbenzene, a second equivalent of benzene coordinates to the coordinatively unsaturated $\text{M-CH}_2\text{CH}_2\text{Ph}$ complex, and subsequent benzene C–H activation affords free ethylbenzene and a new M-Ph complex.

For the $[(^{\text{t}}\text{bpy})\text{Pt}]^+$ catalyst, the difference in energy between these two pathways was calculated to be 4.5 kcal/mol. For the Rh complex, the energy difference between the two pathways is 12.6 kcal/mol. Thus, the calculations predict a greater predilection toward styrene formation for $(^{\text{Fl}}\text{DAB})\text{Rh}$ vs $[(^{\text{t}}\text{bpy})\text{Pt}]^+$, which is consistent with experimental results.¹⁷ Interestingly, the calculations reveal that energy differences for benzene C–H activation ($\Delta\Delta G^\ddagger = 2$ kcal/mol) and β -hydride elimination ($\Delta\Delta G^\ddagger = 0.2$ kcal/mol), the two key steps for the

formation of ethylbenzene and styrene, respectively, are small and likely cannot be used to rationalize the switch in selectivity between $(^{\text{Fl}}\text{DAB})\text{Rh}$ and $[(^{\text{t}}\text{bpy})\text{Pt}]^+$. Rather, it appears that the propensity toward styrene dissociation is the key parameter, with calculated ΔG values for styrene dissociation of 11.8 kcal/mol for $(^{\text{Fl}}\text{DAB})\text{Rh}$ and a surprisingly much larger 27.4 kcal/mol for $[(^{\text{t}}\text{bpy})\text{Pt}]^+$.

Thus, we propose that both $(^{\text{Fl}}\text{DAB})\text{Rh}$ and $[(^{\text{t}}\text{bpy})\text{Pt}]^+$ likely undergo β -hydride elimination from $\text{M}-\text{CH}_2\text{CH}_2\text{Ph}$ intermediates, but for $[(^{\text{t}}\text{bpy})\text{Pt}]^+$ this process is reversible because the energetics for styrene dissociation are too unfavorable. We have reported evidence for reversible β -hydride elimination for ethylbenzene formation by $\text{TpRu}(\text{CO})(\text{NCMe})(\text{Ph})$ (Tp = hydridotris(pyrazolyl)borate).¹³ We note that the formation of diethylbenzenes by $[(^{\text{t}}\text{bpy})\text{Pt}]^+$ is explained by a similar rationale.¹⁷ That is, dissociation of ethylbenzene from $[(^{\text{t}}\text{bpy})\text{Pt}(\text{Ph})(\text{ethylbenzene})]^+$ is slow (relatively), which allows a second arene C–H activation (ultimately leading to diethylbenzenes) to compete with the dissociation of ethylbenzene. More difficult to explain are the calculations for $[(^{\text{t}}\text{bpy})\text{Pt}]^+$, which predict styrene formation over ethylbenzene formation with a $\Delta\Delta G^\ddagger$ of 4.5 kcal/mol, which can arise from the functional and basis sets chosen. Previous calculations and experiments on dipyriddy-supported Pt(II) catalysts^{17,19–21} show that a subtle balance of factors discriminate ethylbenzene from styrene formation. Nonetheless, the present calculations are consistent with the experimental observation of much greater propensity for the latter for Rh(I) versus Pt(II).

Kinetic and Mechanistic Studies. We studied the kinetics of catalysis using **1-OAc** and copper(II) pivalate $[\text{Cu}(\text{OPiv})_2]$. The oxidant $\text{Cu}(\text{OPiv})_2$ was used due to its solubility in benzene. The concentration of ethylene dissolved in benzene was determined according to the method described by Holder and Macauley.⁴⁵ To determine the order of the reaction in **1-OAc**, ethylene, and $\text{Cu}(\text{OPiv})_2$, three sets of kinetic experiments were conducted in which the concentrations of two of the compounds were held constant while one was varied. Observed rate constants (k_{obs}) were extracted from linear fits of the initial rate regime (linear region where likely no catalyst deactivation was occurring) of $[\text{styrene}]$ vs time plots. Due to the complex nature of Rh in solution, the slopes of linear fits were used as k_{obs} without extracting the $[\text{Rh}]$. Log–log plots were used to determine the order of the reaction in each of the compounds examined (Figure 7).

A first-order dependence on ethylene concentration is observed over a concentration range from 79 mM to 237 mM (Figure 7B). While the first-order dependence on ethylene is consistent with the previously reported dependence of apparent TOF on ethylene pressure for catalysis with **1-TFA**,³¹ it is in contrast to previously reported Pt(II)- and Ru(II)-based hydroarylation catalysts. The rate of catalysis with these complexes shows an inverse dependence on the concentration of ethylene, which is due to the formation of $\text{M}(\text{CH}_2\text{CH}_2\text{Ph})(\eta^2\text{-C}_2\text{H}_4)$ intermediates (M = $\text{TpRu}(\text{CO})$ or $[(^{\text{t}}\text{bpy})\text{Pt}]^+$), which were identified as off-cycle resting states.^{13,15,17} An Ir-based olefin hydroarylation catalyst shows a bell-curve dependence on the concentration of ethylene, exhibiting first-order kinetics at low concentrations and inverse first-order kinetics at higher concentrations.²⁴ The observed first-order dependence on $[\text{C}_2\text{H}_4]$ for catalysis with **1-OAc** is consistent with a different resting state from our Pt(II) and Ru(II) catalysts. In fact, for catalysis with **1-OAc**, the energy of the

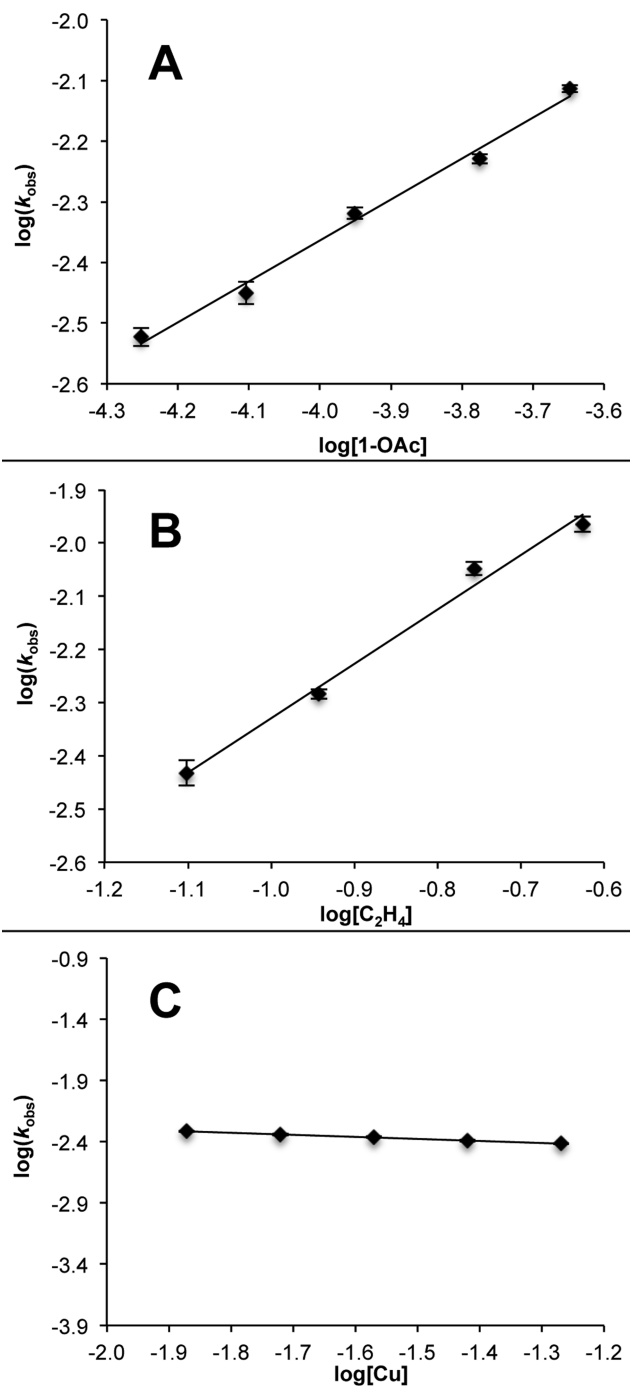


Figure 7. Log–log plots of observed rate constants as a function of (A) concentration of **1-OAc** (slope = 0.66(2), $R^2 = 0.99$). Reaction conditions: 20 mL C_6H_6 , 26.9 mM $\text{Cu}(\text{OPiv})_2$, 50 psig C_2H_4 , 150 °C. (B) Concentration of C_2H_4 (slope = 1.02(8), $R^2 = 0.99$). Reaction conditions: 0.11 mM **1-OAc**, 20 mL C_6H_6 , 13.4 mM $\text{Cu}(\text{OPiv})_2$, 150 °C. (C) Concentration of $\text{Cu}(\text{OPiv})_2$ (slope = $-0.17(2)$, $R^2 = 0.99$). Reaction conditions: 0.11 mM **1-OAc**, 20 mL C_6H_6 , 50 psig C_2H_4 , 150 °C. Each data point represents the average of two independent catalytic reactions, each analyzed in duplicate by GC/FID. Error bars represent the standard deviation of all four values.

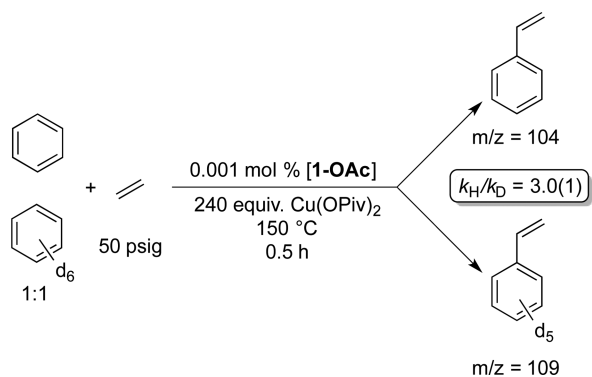
$(^{\text{Fl}}\text{DAB})\text{Rh}(\text{CH}_2\text{CH}_2\text{Ph})(\eta^2\text{-C}_2\text{H}_4)$ complex, which is the analog of the proposed resting states for the Pt(II) and Ru(II) catalysts,^{13,17} is calculated to be higher than that of **1-OAc** by 7.6 kcal/mol.

The log–log plot for $\text{Cu}(\text{OPiv})_2$ (Figure 7C) shows a near zero-order dependence {slope = $-0.17(2)$ } on $[\text{Cu}(\text{OPiv})_2]$ over a concentration range from 13 mM to 54 mM. Given that the involvement of $\text{Cu}(\text{II})$ occurs after the proposed rate-limiting step (*vide infra*), a zero-order dependence is expected. This type of mechanism has been reported for similar oxidative processes, and has been shown to exhibit a zero-order dependence on oxidant.⁴⁶ The slight negative slope indicates that $\text{Cu}(\text{II})$ might suppress catalytic activity. The need for $\text{Cu}(\text{II})$ as an oxidant, but the apparent need of access to low valent $\text{Rh}(\text{I})$ for C–H activation sets up a difficult balance. Thus, one possible explanation of the slight inverse dependence on $\text{Cu}(\text{II})$ concentration is that $\text{Cu}(\text{II})$ oxidizes a $\text{Rh}(\text{I})$ intermediate, pulling it out of the catalytic cycle, but that the equilibrium favors $\text{Rh}(\text{I})$, but the slight magnitude of the apparent inhibition makes it difficult to draw a definitive conclusion.

The log–log plot for **1-OAc** reveals a slope of $0.66(2)$, which is between first-order and half-order (Figure 7A). Further studies showed that the dependence of the reaction rate on **1-OAc** is complicated, varying between first- and half-order as a function of both the concentration of C_2H_4 and temperature (see Supporting Information for plots). The order in Rh was determined over a concentration range from 0.056 to 0.23 mM at three different concentrations of C_2H_4 , and, in a separate series of experiments, the order in **1-OAc** was determined at three different temperatures. With $[\text{C}_2\text{H}_4]$ variation, the order in Rh varied exhibiting close to half-order kinetics at lower $[\text{C}_2\text{H}_4]$ {at 7.9 mM C_2H_4 , reaction order in **1-OAc** = $0.58(3)$ } and close to first order kinetics at higher $[\text{C}_2\text{H}_4]$ {at 17.5 mM C_2H_4 , reaction order in **1-OAc** = $0.96(1)$ }. The order in Rh was found to vary inversely with temperature, exhibiting closer to first-order kinetics at lower temperatures {at 130 °C, order in **1-OAc** = $0.83(1)$ } and closer to half-order kinetics at higher temperatures {at 160 °C, order in **1-OAc** = $0.64(1)$ }. Limitations of the catalytic process make kinetic studies outside of this temperature range challenging. These results indicate the possibility of competing catalytic pathways (*vide infra*).

The kinetic isotope effect (KIE) for catalysis using C_6H_6 vs C_6D_6 was determined using two methods. In one experiment, catalysis was performed using an equimolar mixture of per-protio and per-deutero benzene (Scheme 4). After 30 min, a $k_{\text{H}}/k_{\text{D}}$ of $3.0(1)$ was observed upon comparison of the peaks for

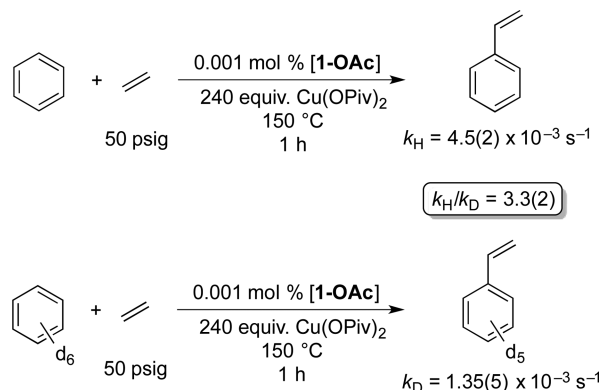
Scheme 4. Kinetic Isotope Experiment Using a 1:1 Molar Mixture of C_6H_6 : C_6D_6 ^a



^a $k_{\text{H}}/k_{\text{D}}$ value represents the average of three independent catalytic reactions, each analyzed in triplicate by GC/MS. Reported error represents the standard deviation of all nine values.

per-protio styrene ($m/z = 104$) and styrene- d_5 ($m/z = 109$) by mass spectrometry. In a separate series of reactions, catalysis was performed in C_6H_6 and C_6D_6 independently (Scheme 5). A

Scheme 5. Kinetic Isotope Experiment Using Independent Reactions in C_6H_6 and C_6D_6 ^a



^a k_{H} and k_{D} values were determined using the method of initial rates for two independent catalytic reactions each, with all samples analyzed in duplicate by GC/FID. The reported error represents the propagated standard deviation of all values and linear regressions.

$k_{\text{H}}/k_{\text{D}}$ of $3.3(2)$ was determined for these reactions using k_{obs} values calculated after 1 h of reaction. The two $k_{\text{H}}/k_{\text{D}}$ values are statistically identical (for more discussion of KIEs for catalysis, *vide infra*). The KIEs are consistent with reported values for C–H activation by d^8 complexes, which often exhibit KIE values of ≥ 2.5 .^{47,48} It is also important to note that d_{6-8} products were not observed except those predicted by the natural abundance of deuterium in ethylene.

We also sought to probe the reversibility of the benzene C–H activation step through benzene H/D exchange experiments. A solution of **1-OAc** (0.001 mol %) and $\text{Cu}(\text{OPiv})_2$ (120 equiv) in a 1:1 molar mixture of C_6H_6 and C_6D_6 was heated to 150 °C. The isotopic distribution of benzene was determined by GC/MS for the initial solution prior to heating, after 4 h of heating, and after 24 h of heating. No change was observed in the isotopic distribution. To determine whether the acetic acid generated in the catalytic cycle could contribute to the reversibility of benzene C–H activation, a solution of **1-OAc** (0.001 mol %), $\text{Cu}(\text{OPiv})_2$ (120 equiv), and $\text{CD}_3\text{CO}_2\text{D}$ (500 equiv) in C_6H_6 was heated to 150 °C. The isotopic distribution of benzene was determined by GC/MS for the initial solution prior to heating, after 4 h of heating, and after 24 h of heating with no change observed.

To determine if the equilibrium between monomer and dimer plays a role in benzene C–H activation, ethylene was added to H/D exchange reactions as experiments show that only monomer exists in the presence of ethylene. A solution of **1-OAc** (0.001 mol %), $\text{Cu}(\text{OPiv})_2$ (120 equiv), ethylene (50 psig), and $\text{CD}_3\text{CO}_2\text{D}$ (500 equiv) in C_6H_6 was heated to 150 °C. The isotopic distribution of benzene was determined by GC/MS for the initial solution prior to heating, after 4 h of heating, and after 24 h of heating, and no change was observed over time. The isotopic distribution of the reaction product, styrene was also determined by GC/MS. Comparing the isotopic distribution in the reaction after 4 and 24 h to the MS of an authentic standard, the amount of styrene- d_1 increased by $\sim 5\%$ over the course of the reaction. This indicates that the acid could be catalyzing H/D exchange with styrene, but the

KIE of 6.7(6) in the first-order regime. Within deviation of the data, these results are consistent with the proposed reaction pathways.

To further probe our proposed mechanism, experiments were run at high $[C_2H_4]$ in an attempt to observe saturation kinetics (Figure 9). At concentrations less than 237 mM, a first-

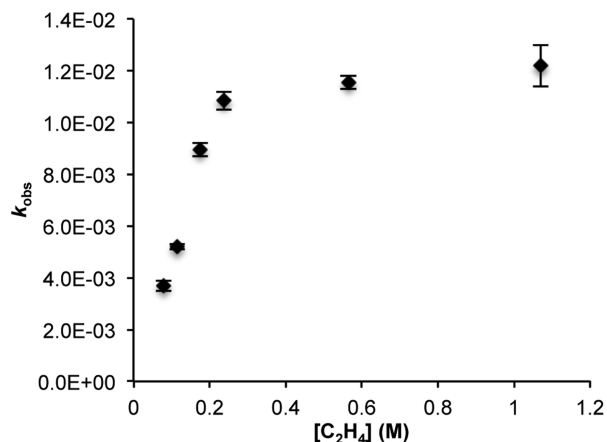


Figure 9. Plot of k_{obs} vs $[C_2H_4]$. Reaction conditions: 0.11 mM 1-OAc, 20 mL C_6H_6 , 13.4 mM $Cu(OPiv)_2$, 150 °C. Each data point represents the average of two independent catalytic reactions, each analyzed in duplicate by GC/FID. Error bars represent the standard deviation of all four values.

order dependence on ethylene is observed, but above 237 mM, saturation is observed. In an attempt to observe the inverse dependence on acid (HX) predicted by the proposed rate law, catalysis with 1-OAc was performed in the presence of added AcOH (500 and 1000 equiv relative to 1-OAc). Using initial rates, we found that the rate of catalysis is suppressed by AcOH (Figure 10). This is consistent with the limiting form for the low $[C_2H_4]$ regime.

It is important to note that while the inverse dependence on acid would predict inhibition as the reaction proceeds, this is

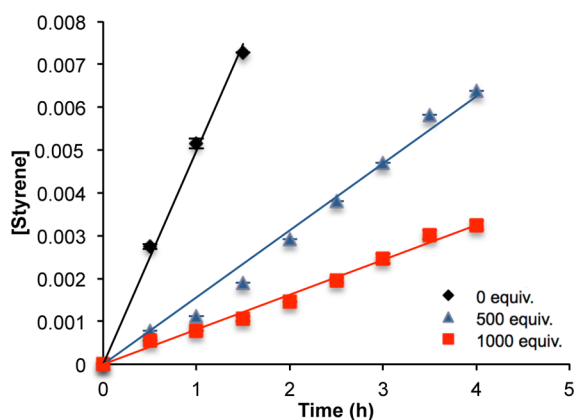


Figure 10. [Styrene] vs time plot for the initial rate regime of catalysis with 1-OAc upon the addition of 0 equiv (slope = 0.005, $R^2 = 0.99$), 500 equiv (slope = 0.0016, $R^2 = 0.99$), and 1000 equiv (slope = 0.0008, $R^2 = 0.99$) of AcOH relative to the concentration of 1-OAc. Reaction conditions: 20 mL C_6H_6 , 13.4 mM $Cu(OPiv)_2$, 50 psig C_2H_4 , AcOH (0, 500, or 1000 equiv relative to 1-OAc), 150 °C. Each data point represents the average of two independent catalytic reactions, each analyzed in duplicate by GC/FID. Error bars represent the standard deviation of all four values.

not observed under the catalytic conditions we tested. This is likely due to the low concentration of acid in solution under the conditions tested. The limiting form for the high $[C_2H_4]$ regime predicts a zero-order dependence on acid (HX), so catalysis was performed at 400 psig C_2H_4 with 0, 500, and 1000 equiv of AcOH added (relative to Rh). At this high concentration of ethylene, the observed rate of reaction without added AcOH is statistically identical to that of catalytic experiments with added acid, which is consistent with the proposed reaction pathway. Rationalization of the change in the dependence on Rh as temperature is variation is more difficult since the route that is first-order in Rh involves a series of ill-defined reactions with Cu(II). But, it is not surprising that the contribution of the two competing pathways varies with temperature.

SUMMARY AND CONCLUSIONS

The complex $(^{F1}DAB)Rh(OAc)(\eta^2-C_2H_4)$ is an effective catalyst for the direct conversion of benzene, ethylene and Cu(II) oxidant to styrene. This Rh catalyst precursor is unique for its selectivity for styrene formation as well as catalyst longevity. The mechanism of this reaction has been studied and compared to both electron-rich Ru(II) and related electrophilic cationic Pt(II) catalysts. Based on these results, the following conclusions can be drawn:

- (1) Combined experimental and computational studies are consistent with catalysis that proceeds through benzene C–H activation, displacement of coordinated acetic acid by ethylene, rate-limiting insertion of ethylene into the Rh–Ph bond, and β -hydride elimination followed by liberation of styrene and reaction with Cu(II) (*vide infra*, comment (3), for additional comments).
- (2) The apparent induction period observed for catalysis with $(^{F1}DAB)Rh(TFA)(\eta^2-C_2H_4)$ is not likely the result of *in situ* formation of insoluble Rh nanoparticles as the active catalyst. Rather, $(^{F1}DAB)Rh(TFA)(\eta^2-C_2H_4)$ converts to $(^{F1}DAB)Rh(OAc)(\eta^2-C_2H_4)$ *in situ*, which catalyzes styrene production at a faster rate than the TFA analog. The difference in rate of catalysis for 1-OAc and 1-TFA is likely a result of the difference in ground state energies rather than OAc/TFA influence on transition states, since the proposed rate-determining step occurs once the carboxylate ligands are completely dissociated.
- (3) A mechanism for catalysis with $(^{F1}DAB)Rh(X)(\eta^2-C_2H_4)$ (X = OAc or TFA) has been proposed that involves two pathways whose contributions vary with $[C_2H_4]$ and temperature. Accordingly, the derived rate law predicts different behavior at low and high $[C_2H_4]$. At low $[C_2H_4]$, the limiting form predicts half-order in [Rh], first-order in ethylene, zero-order in Cu, and an inverse dependence on acid concentration. At high $[C_2H_4]$, the limiting form predicts first-order in [Rh], and zero-order dependence on all others. Saturation behavior has been observed for ethylene, and the rate of reaction is suppressed in the presence of added acid at low $[C_2H_4]$ but not at high $[C_2H_4]$, both results are consistent with the proposed mechanism and rate law. The kinetics are also consistent with computational modeling, which predicts rate-limiting ethylene insertion into the Rh–Ph bond. However, alternative explanations of the kinetic data are possible, such as inhibition of

catalysis upon reaction of the catalyst with acid (to remove Rh from the catalytic cycle) that is influenced by concentration of ethylene. Despite other possible explanations for this complex catalytic process, our mechanistic proposal is consistent with both experimental and computational data and, we believe, is the mechanistic model that is most consistent with the data.

- (4) The selectivity for styrene production (versus ethylbenzene) using $(^{\text{F}}\text{DAB})\text{Rh}(\text{X})(\eta^2\text{-C}_2\text{H}_4)$ appears to result from more favorable styrene dissociation compared to related cationic Pt(II) catalysts.

EXPERIMENTAL SECTION

General Considerations. All manipulations were performed under an atmosphere of dry nitrogen using standard Schlenk or high-vacuum techniques and/or in a Vac Atmospheres Dri-Lab glovebox equipped with a Dri-Train MO-41 purifier. Dry, oxygen-free solvents were employed throughout. Benzene was dried by passage through columns of activated alumina. THF was dried by passage through columns of activated alumina, followed by distillation from sodium benzophenone ketyl. Pentane was dried over sodium benzophenone ketyl. Deuterated solvents were purchased from Cambridge Isotope Labs, degassed, and dried over molecular sieves. NMR spectra were recorded on a Varian NMRS 600 MHz NMR spectrometer (^{19}F , 564.33 MHz operating frequency), Bruker Avance III 600 MHz NMR spectrometer (^1H , 600.13 MHz operating frequency), or a Bruker Avance III 800 MHz NMR spectrometer (^{13}C , 201.27 MHz operating frequency), and are reported with reference to residual solvent resonances. GC/MS was performed using a Shimadzu GCMS-QP2010 Plus system with a 30 m \times 0.25 mm SHRXI-5MS column with 0.25 μm film thickness using electron impact (EI) ionization. GC/FID was performed using a Shimadzu GC-2014 system with a 30 m \times 0.25 mm HP5 column with 0.25 μm film thickness. Infrared spectra were collected on a Shimadzu IRAffinity-1 FT-IR instrument using KBr pellets.

Styrene production was quantified using linear regression analysis of gas chromatograms of standard samples of authentic product. A plot of peak area ratios versus molar ratios gave a regression line. For the GC/FID system, the slope and correlation coefficient of the regression line were 1.34 and 0.99, respectively. Ethylene was purchased in gas cylinders from GTS-Welco and used as received. All other reagents were purchased from commercial sources and used as received. $[\text{Rh}(\eta^2\text{-C}_2\text{H}_4)_2(\mu\text{-Cl})_2]$ was prepared according to literature procedures.⁵⁰ $[\text{Rh}(\eta^2\text{-C}_2\text{H}_4)_2(\mu\text{-TFA})_2]$ was prepared using an adaptation of literature procedures, substituting AgTFA for TITFA.⁵¹ While the synthesis of $[\text{Rh}(\eta^2\text{-C}_2\text{H}_4)_2(\mu\text{-OAc})_2]$ has been reported previously,⁵² higher yields were obtained by using the same method as for the synthesis of $[\text{Rh}(\eta^2\text{-C}_2\text{H}_4)_2(\mu\text{-TFA})_2]$,⁵¹ substituting TIOAc for TITFA. $^{\text{F}}\text{DAB}$ was synthesized according to literature procedures.⁵³ Copper(II) pivalate $[\text{Cu}(\text{OPiv})_2]$ was synthesized according to literature procedures.⁵⁴ Procedures for catalytic reactions using 1-TFA have been reported previously.³¹ The Maitlis filtration test was performed according to the previously reported procedure.³⁵

Procedure for TEM/EDS Experiments. Transmission electron microscopy images were obtained using a JEOL 2000FX-II electron microscope equipped with a Gresham high-angle X-ray detector. An accelerating voltage of 200 kV was used with a resolution of 1.4 Å. Energy-dispersive X-ray spectroscopy (EDS) data were used to detect the presence of Rh and Cu, and were collected using an incident beam diameter of approximately 25 nm. Samples for electron microscopy were prepared by ultrasonic dispersion in 1,4-dioxane followed by deposition onto a holey carbon film supported on a 400 mesh Cu grid. Samples were allowed to dry in air for 24 h before insertion into the microscope vacuum chamber.

Computational Methods. Density functional theory (DFT) was applied to the study of styrene formation using both 1-TFA and 1-OAc. The Gaussian 09 package was used to perform all simulations.⁵⁵ All stationary points were obtained using the B3LYP^{56,57} functional

along with the LANL2DZ pseudopotential basis set for Rh and the 6-31G(d) basis set for main group elements; the 6-311++G(d,p) pseudopotential basis set was used on main group elements for single point calculations at the B3LYP/LANL2DZ+6-31G(d) stationary points. Free energies are reported in kcal/mol at 423.15 K assuming a pressure of 1 atm. Unscaled B3LYP/LANL2DZ+6-31G(d) vibrational frequencies were used for the enthalpic and entropic corrections. The GD3BJ dispersion correction⁵⁸ and the SMD solvation model⁵⁹ were utilized in the presence of benzene as the continuum solvent on the single-point calculations. Stationary points were differentiated as minima or transition states based on the number of imaginary frequencies (zero or one, respectively) calculated based on the energy Hessian.

The monomer/dimer equilibrium of both 1-TFA and 1-OAc was also examined using DFT. All stationary points were obtained using the M06⁶⁰ functional along with the LANL2DZ pseudopotential basis set for Rh and the 6-31G(d) basis set for main group elements; the 6-311++G(d,p) pseudopotential basis set was used on main group elements for single-point calculations at the M06/LANL2DZ+6-31G(d) stationary points. Free energies are reported in kcal/mol at 423.15 K, assuming a pressure of 1 atm. Unscaled M06/LANL2DZ+6-31G(d) vibrational frequencies were used for the enthalpic and entropic corrections. The SMD solvation model⁵⁹ was utilized in the presence of benzene as the continuum solvent on the single-point calculations.

Synthesis of $(^{\text{F}}\text{DAB})\text{Rh}(\text{OAc})(\eta^2\text{-C}_2\text{H}_4)$ [1-OAc]. To a stirring solution of $[\text{Rh}(\eta^2\text{-C}_2\text{H}_4)_2(\mu\text{-OAc})_2]$ (200 mg, 0.459 mmol) in THF (20 mL), $^{\text{F}}\text{DAB}$ (382 mg, 0.918 mmol) was added, and the mixture was stirred for 30 min. The solvent was removed *in vacuo*, and the purple solid was washed with pentane (ca. 80 mL) and dried to afford 1 as a purple powder (218 mg, 0.360 mmol, 40%). Upon prolonged drying *in vacuo*, the ethylene is removed to form $[(^{\text{F}}\text{DAB})\text{Rh}(\mu\text{-OAc})_2]$ (1D-OAc), the characterization data for which are as follows. ^1H NMR (600.13 MHz, C_6D_6): δ 1.75 (s, 6H, COOCH_3), -0.95 (s, 12H, DAB- CH_3). ^{13}C NMR (201.27 MHz, C_6D_6): δ 186.0 (s, COOCH_3), 163.9 (s, $\text{C}=\text{N}$), 141.2 (m, C_6F_5 -meta C), 140.0 (m, C_6F_5 -meta C), 138.9 (m, C_6F_5 -ortho C), 137.7 (m, C_6F_5 -ortho C), 131.0 (m, C_6F_5 -para C), 130.1 (s, C_6F_5 -ipso C), 22.8 (s, COOCH_3), 19.7 (s, DAB- CH_3). ^{19}F NMR (564.33 MHz, C_6D_6): δ -144.0 (d, $^3J_{\text{FF}} = 23$ Hz, C_6F_5 -ortho F), -151.3 (d, $^3J_{\text{FF}} = 23$ Hz, C_6F_5 -ortho F), -156.6 (t, $^3J_{\text{FF}} = 23$ Hz, C_6F_5 -meta F), -163.1 (t, $^3J_{\text{FF}} = 23$ Hz, C_6F_5 -meta F), -165.9 (t, $^3J_{\text{FF}} = 23$ Hz, C_6F_5 -para F). IR (KBr): 1530, 1497 cm^{-1} (O_2CMe sym and asym). Upon pressurizing with ethylene, 1-OAc can be regenerated, and its *in situ* characterization data are as follows: ^1H NMR (600.13 MHz, C_6D_6): δ 2.5 (broad s, 4H, C_2H_4), 1.68 (s, 3H, COOCH_3), -1.79 (s, 6H, DAB- CH_3).

Reaction of 1-TFA with Ethylbenzene. A stock solution containing 1-TFA (0.112 mM), decane (10 equiv relative to 1-TFA), and ethylbenzene (50 mL) was prepared in a volumetric flask. Fisher-Porter reactors were charged with stock solution (20 mL) and copper acetate (13.4 mM). The vessels were sealed, pressurized with ethylene (50 psig), and stirred while heated to 150 °C. The reactions were sampled at 4, 8, 12, and 24 h. At each time point the reactors were cooled to room temperature, sampled, recharged with ethylene, and reheated. Aliquots of the reaction mixture were analyzed by GC/MS, and products were identified using through a search of the NIST mass spectral database.

Attempted Oxidative Hydrophenylation of Ethylene Using Washed Materials Recovered from Catalysis with 1-TFA and $\text{Cu}(\text{OAc})_2$. Two duplicate catalytic reactions with 1-TFA were run to completion. The resulting mixtures were combined and dried *in vacuo*. The solid was sonicated in 1,4-dioxane for 30 min, after which the solution was decanted leaving only insoluble materials, which were dried *in vacuo*. Two Fisher-Porter reactors were each charged with half of the recovered material, decane (4 μL , 0.022 mmol), benzene (20 mL), and $\text{Cu}(\text{OAc})_2$ (49 mg, 0.27 mmol). The vessels were sealed, pressurized with ethylene (50 psig), and stirred while heated to 150 °C. The reactions were sampled at 4 and 24 h. At each time point the reactors were cooled to room temperature, sampled, recharged with ethylene, and reheated. Aliquots of the reaction mixture were analyzed

by GC/FID using relative peak area vs an internal standard (decane). No styrene was observed after 24 h of heating.

Oxidative Hydrophenylation of Ethylene Using 1-OAc. A representative catalytic reaction is described. A stock solution containing 1-OAc (3.4 mg, 0.0056 mmol), decane (11 μ L, 0.056 mmol), and benzene (50 mL) was prepared in a volumetric flask. Fisher-Porter reactors were charged with stock solution (20 mL) and Cu(OAc)₂ (49 mg, 0.27 mmol). The vessels were sealed, pressurized with ethylene (25 psig), and stirred while heated to 150 °C. The reactions were sampled every hour until complete. At each time point the reactors were cooled to room temperature, sampled, recharged with ethylene, and reheated. Aliquots of the reaction mixture were analyzed by GC/FID using relative peak area vs an internal standard (decane).

Oxidative Hydrophenylation of Ethylene as a Function of [C₂H₄]. A stock solution containing 1-OAc (0.112 mM), decane (10 equiv relative to 1-OAc), and benzene (250 mL) was prepared in a volumetric flask. Fisher-Porter reactors (2 reactors per concentration level) were charged with stock solution (20 mL) and copper pivalate (13.4 mM). The vessels were sealed, pressurized with ethylene (35, 50, 75, or 100 psig), and stirred while heated to 150 °C. The reactions were sampled every 30 min until complete. At each time point the reactors were cooled to room temperature, sampled, recharged with ethylene, and reheated. Aliquots of the reaction mixture were analyzed by GC/FID using relative peak area vs an internal standard (decane).

Oxidative Hydrophenylation of Ethylene as a Function of [Cu(OPiv)₂]. A stock solution containing 1-OAc (0.112 mM), decane (10 equiv relative to 1-OAc), and benzene (250 mL) was prepared in a volumetric flask. Fisher-Porter reactors (2 reactors per concentration level) were charged with stock solution (20 mL) and copper pivalate (13.4, 19.0, 26.9, 38.1, or 53.8 mM). The vessels were sealed, pressurized with ethylene (50 psig), and stirred while heated to 150 °C. The reactions were sampled every 30 min until complete. At each time point the reactors were cooled to room temperature, sampled, recharged with ethylene, and reheated. Aliquots of the reaction mixture were analyzed by GC/FID using relative peak area vs an internal standard (decane).

Oxidative Hydrophenylation of Ethylene as a Function of [1-OAc]. Five separate stock solutions were prepared in 50 mL volumetric flasks, each containing 1-OAc (0.225, 0.168, 0.112, 0.079, or 0.056 mM), decane (10 equiv relative to 1-OAc), and benzene (50 mL). Fisher-Porter reactors (2 reactors per concentration level) were charged with stock solution (20 mL) and copper pivalate (26.9 mM). The vessels were sealed, pressurized with ethylene (50 psig), and stirred while heated to 150 °C. The reactions were sampled every 30 min until complete. At each time point the reactors were cooled to room temperature, sampled, recharged with ethylene, and reheated. Aliquots of the reaction mixture were analyzed by GC/FID using relative peak area vs an internal standard (decane).

Dependence of Order in [1-OAc] on [C₂H₄]. Three separate stock solutions were prepared in 50 mL volumetric flasks, each containing 1-OAc (0.225 mM, 0.112 mM, or 0.056 mM), decane (10 equiv relative to 1-OAc), and benzene (50 mL). Fisher-Porter reactors (6 reactors per concentration of Rh) were charged with stock solution (20 mL) and copper pivalate (26.9 mM). The vessels were sealed, pressurized with ethylene (35 psig, 50 psig, or 75 psig; 2 reactors per pressure at each Rh concentration), and stirred while heated to 150 °C. The reactions were sampled every 30 min until complete. At each time point the reactors were cooled to room temperature, sampled, recharged with ethylene, and reheated. Aliquots of the reaction mixture were analyzed by GC/FID using relative peak area vs an internal standard (decane).

Dependence of Order in [1-OAc] on Temperature. Three separate stock solutions were prepared in 50 mL volumetric flasks, each containing 1-OAc (0.225 mM, 0.112 mM, or 0.056 mM), decane (10 equiv relative to 1-OAc), and benzene (50 mL). Fisher-Porter reactors (6 reactors per concentration of Rh) were charged with stock solution (20 mL) and copper pivalate (26.9 mM). The vessels were sealed, pressurized with ethylene (to keep the concentration of ethylene dissolved in solution constant across all temperatures,

different pressures were used, all of which correspond to 114 mM C₂H₄: 30 psig for 130 °C reactions, 50 psig for 150 °C reactions, or 60 psig for 160 °C reactions; 2 reactors per pressure at each Rh concentration), and stirred while heated to 130 °C, 150 °C, or 160 °C. The reactions were sampled every 30 min until complete. At each time point the reactors were cooled to room temperature, sampled, recharged with ethylene, and reheated. Aliquots of the reaction mixture were analyzed by GC/FID using relative peak area vs an internal standard (decane).

H/D Exchange Experiments—1:1 Ratio of C₆H₆ to C₆D₆. A stock solution containing 1-OAc (0.112 mM), Cu(OPiv)₂ (13.4 mM), and a 1:1 molar mixture of C₆H₆ and C₆D₆ (25 mL) was prepared in a volumetric flask. PTFE-valved reaction tubes were charged with stock solution (10 mL), sealed, and heated to 150 °C. The reactions were sampled at 4 and 24 h. At each time point the reactors were cooled to room temperature, sampled, and reheated. Aliquots of the reaction mixture were analyzed by GC/MS. The isotopic distribution of benzene-*d_n* (*n* = 0–6) was measured for the initial stock solution and at each time point.

H/D Exchange Experiments—500 equiv CD₃COOD. A stock solution containing 1-OAc (0.112 mM), Cu(OPiv)₂ (13.4 mM), CD₃COOD (56 mM), and C₆H₆ (25 mL) was prepared in a volumetric flask. PTFE-valved reaction tubes were charged with stock solution (10 mL), sealed, and heated to 150 °C. The reactions were sampled at 4 and 24 h. At each time point the reactors were cooled to room temperature, sampled, and reheated. Aliquots of the reaction mixture were analyzed by GC/MS. The isotopic distribution of benzene-*d_n* (*n* = 0–6) was measured for the initial stock solution and at each time point.

H/D Exchange Experiments—500 equiv CD₃COOD with Added Ethylene. A stock solution containing 1-OAc (0.112 mM) and C₆H₆ (25 mL) was prepared in a volumetric flask. Fisher-Porter reactors were charged with stock solution (10 mL), copper pivalate (13.4 mM), and CD₃COOD (56 mM). The vessels were sealed, pressurized with ethylene (50 psig), and stirred while heated to 150 °C. The reactions were sampled at 4 and 24 h. At each time point the reactors were cooled to room temperature, sampled, and reheated. Aliquots of the reaction mixture were analyzed by GC/MS. The isotopic distribution of benzene-*d_n* (*n* = 0–6) was measured for the initial stock solution and at each time point. The isotopic distribution of styrene-*d_n* (*n* = 0–8) was also measured at each time point.

Kinetic Isotope Effect Experiments using a 1:1 Molar Mixture of C₆H₆ and C₆D₆. A stock solution containing 1-OAc (0.112 mM) and a 1:1 molar mixture of C₆H₆ and C₆D₆ (100 mL) was prepared in a volumetric flask. For reactions at 35 and 50 psig, Fisher-Porter reactors were charged with stock solution (10 mL) and Cu(OPiv)₂ (240 equiv relative to 1-OAc). The vessels were sealed, pressurized with ethylene (50 psig), and stirred while heated to 150 °C. The reactions were sampled at 30 min and at 1, 2, and 3 h. At each time point the reactors were cooled to room temperature, sampled, recharged with ethylene, and reheated. For reactions at 150 psig, stainless steel high-pressure reactors equipped with glass liners were charged with stock solution (10 mL) and Cu(OPiv)₂ (240 equiv relative to 1-OAc). The vessels were sealed, pressurized with ethylene (150 psig), and stirred while heated to 150 °C. The reactions were sampled at 30 min, 1, 2, and 3 h. At each time point the reactors were sampled at temperature using a narrow bore dip tube. Aliquots of the reaction mixture were analyzed by GC/MS. KIE was determined by examining the ratio of styrene (*m/z* = 104) to styrene-*d₅* (*m/z* = 109) in the mass spectrum, accounting for the initial isotopic distribution and natural abundance. No change in the isotopic distribution for benzene was observed over the course of the reaction, and the observed isotopic distribution of product was consistent with the initial distribution. No *d_{6–8}* products were observed, except those predicted by the natural abundance of deuterium in ethylene.

Oxidative Hydrophenylation of Ethylene Using 1-OAc in C₆D₆. A stock solution containing 1-OAc (0.112 mM), decane (10 equiv relative to 1-OAc), and C₆D₆ (50 mL) was prepared in a volumetric flask. Fisher-Porter reactors were charged with stock solution (20 mL) and copper pivalate (26.9 mM). The vessels were

sealed, pressurized with ethylene (50 psig), and stirred while heated to 150 °C. The reactions were sampled every 30 min for 3 h. At each time point the reactors were cooled to room temperature, sampled, recharged with ethylene, and reheated. Aliquots of the reaction mixture were analyzed by GC/FID using relative peak area vs an internal standard (decane).

Oxidative Hydrophenylation of Ethylene Using *in Situ* Generated $(\text{F}^{\text{t}}\text{DAB})\text{RhCl}_3(\eta^2\text{-C}_2\text{H}_4)$. A stock solution containing RhCl_3 (0.112 mM), $\text{F}^{\text{t}}\text{DAB}$ (0.112 mM), decane (1.12 mM), and benzene (50 mL) was prepared in a volumetric flask. Fisher-Porter reactors were charged with stock solution (20 mL) and $\text{Cu}(\text{OPiv})_2$ (27 mM). The vessels were sealed, pressurized with ethylene (50 psig), and stirred while heated to 150 °C. The reactions were sampled at 4 and 24 h. At each time point the reactors were cooled to room temperature, sampled, recharged with ethylene, and reheated. Aliquots of the reaction mixture were analyzed by GC/FID using relative peak area vs an internal standard (decane).

Oxidative Hydrophenylation of Ethylene Using 1-OAc at Pressures >100 psig. A representative catalytic reaction is described. A stock solution containing 1-OAc (0.112 mM), decane (1.12 mM), and benzene (50 mL) was prepared in a volumetric flask. Stainless steel high pressure reactors equipped with glass liners were charged with stock solution (10 mL) and $\text{Cu}(\text{OPiv})_2$ (27 mM). The vessels were sealed, pressurized with ethylene (400 psig), and stirred while heated to 150 °C. The reactions were sampled every hour until complete. At each time point the reactors were sampled at temperature using a narrow bore dip tube. Aliquots of the reaction mixture were analyzed by GC/FID using relative peak area vs an internal standard (decane).

Oxidative Hydrophenylation of Ethylene Using 1-OAc with Added AcOH at Low Pressures <100 psig. A representative catalytic reaction is described. A stock solution containing 1-OAc (0.112 mM), decane (1.12 mM), and benzene (50 mL) was prepared in a volumetric flask. Fisher-Porter reactors were charged with stock solution (20 mL), AcOH (56 mM), and $\text{Cu}(\text{OPiv})_2$ (27 mM). The vessels were sealed, pressurized with ethylene (50 psig), and stirred while heated to 150 °C. The reactions were sampled every 30 min until complete. At each time point the reactors were cooled to room temperature, sampled, recharged with ethylene, and reheated. Aliquots of the reaction mixture were analyzed by GC/FID using relative peak area vs an internal standard (decane).

Oxidative Hydrophenylation of Ethylene Using 1-OAc with Added AcOH at High Pressures >100 psig. A representative catalytic reaction is described. A stock solution containing 1-OAc (0.112 mM), decane (1.12 mM), and benzene (50 mL) was prepared in a volumetric flask. Stainless steel high pressure reactors equipped with glass liners were charged with stock solution (10 mL), AcOH (56 mM), and $\text{Cu}(\text{OPiv})_2$ (27 mM). The vessels were sealed, pressurized with ethylene (400 psig), and stirred while heated to 150 °C. The reactions were sampled every 30 min until complete. At each time point the reactors were sampled at temperature using a narrow-bore dip tube. Aliquots of the reaction mixture were analyzed by GC/FID using relative peak area vs an internal standard (decane).

■ ASSOCIATED CONTENT

📄 Supporting Information

The Supporting Information is available free of charge on the ACS Publications website at DOI: [10.1021/jacs.6b10658](https://doi.org/10.1021/jacs.6b10658).

Initial rate plots for catalytic reactions, kinetic derivations, mass spectra, and TEM images, including Figures S1–S17 (PDF)

Full computational results for B3LYP (XYZ)

Full computational results for M06 (XYZ)

■ AUTHOR INFORMATION

Corresponding Authors

*t@unt.edu

*tbg7h@virginia.edu

ORCID

Benjamin A. Vaughan: [0000-0001-9607-5696](https://orcid.org/0000-0001-9607-5696)

T. Brent Gunnoe: [0000-0001-5714-3887](https://orcid.org/0000-0001-5714-3887)

Notes

The authors declare no competing financial interest.

■ ACKNOWLEDGMENTS

This work was supported by the U.S. Department of Energy, Office of Basic Energy Sciences [DE-SC0000776 (T.B.G.) and DE-FG02-03ER15387 (T.R.C.)], an AES Graduate Fellowship in Energy Research (M.S.W.-G.), and a University of Virginia Jefferson Arts & Sciences Dissertation Year Fellowship (M.S.W.-G.). The authors also thank Prof. Mahdi Abu-Omar and Dr. Mark Pouy for useful discussions.

■ REFERENCES

- (1) Olah, G. A.; Molnár, Á. *Hydrocarbon Chemistry*, 2 ed.; Wiley: Hoboken, NJ, 2003.
- (2) Perego, C.; Pollesel, P. Advances in Aromatics Processing Using Zeolite Catalysts. In *Advances in Nanoporous Materials*; Stefan, E., Ed.; Elsevier: Oxford, 2010; Vol. 1, pp 97.
- (3) Chen, S.-S. Styrene. *Kirk-Othmer Encyclopedia of Chemical Technology*; Wiley: Hoboken, NJ, 2000.
- (4) Wittcoff, H. A.; Reuben, B. G.; Plotkin, J. S. Chemicals and Polymers from Ethylene. *Industrial Organic Chemicals*; Wiley: Hoboken, NJ, 2004; pp 100.
- (5) *Chem Systems, I. Styrene/Ethylbenzene*; Process Evaluation/Research Planning (PERP) Program Report 91-9; Chem Systems, Inc.: New York, 1992.
- (6) Lucchini, M.; Galeotti, A. International Patent WO2007073918A1, 2007.
- (7) Perego, C.; Ingallina, P. *Catal. Today* **2002**, *73*, 3.
- (8) Perego, C.; Ingallina, P. *Green Chem.* **2004**, *6*, 274.
- (9) Čejka, J.; Wichterlová, B. *Catal. Rev.: Sci. Eng.* **2002**, *44*, 375.
- (10) Gerzeliev, I. M.; Khadzhev, S. N.; Sakharova, I. E. *Pet. Chem.* **2011**, *51*, 39.
- (11) *CRC handbook of chemistry and physics*; Weast, R. C., Ed.; CRC Press/Taylor & Francis: Boca Raton, FL, 1977.
- (12) Lail, M.; Arrowood, B. N.; Gunnoe, T. B. *J. Am. Chem. Soc.* **2003**, *125*, 7506.
- (13) Lail, M.; Bell, C. M.; Conner, D.; Cundari, T. R.; Gunnoe, T. B.; Petersen, J. L. *Organometallics* **2004**, *23*, 5007.
- (14) McKeown, B. A.; Foley, N. A.; Lee, J. P.; Gunnoe, T. B. *Organometallics* **2008**, *27*, 4031.
- (15) Foley, N. A.; Lee, J. P.; Ke, Z.; Gunnoe, T. B.; Cundari, T. R. *Acc. Chem. Res.* **2009**, *42*, 585.
- (16) Andreatta, J. R.; McKeown, B. A.; Gunnoe, T. B. *J. Organomet. Chem.* **2011**, *696*, 305.
- (17) McKeown, B. A.; Gonzalez, H. E.; Friedfeld, M. R.; Gunnoe, T. B.; Cundari, T. R.; Sabat, M. *J. Am. Chem. Soc.* **2011**, *133*, 19131.
- (18) Joslin, E. E.; McMullin, C. L.; Gunnoe, T. B.; Cundari, T. R.; Sabat, M.; Myers, W. H. *Organometallics* **2012**, *31*, 6851.
- (19) McKeown, B. A.; Gonzalez, H. E.; Michaelos, T.; Gunnoe, T. B.; Cundari, T. R.; Crabtree, R. H.; Sabat, M. *Organometallics* **2013**, *32*, 3903.
- (20) McKeown, B. A.; Gonzalez, H. E.; Friedfeld, M. R.; Brosnahan, A. M.; Gunnoe, T. B.; Cundari, T. R.; Sabat, M. *Organometallics* **2013**, *32*, 2857.
- (21) McKeown, B. A.; Gonzalez, H. E.; Gunnoe, T. B.; Cundari, T. R.; Sabat, M. *ACS Catal.* **2013**, *3*, 1165.
- (22) McKeown, B. A.; Prince, B. M.; Ramiro, Z.; Gunnoe, T. B.; Cundari, T. R. *ACS Catal.* **2014**, *4*, 1607.
- (23) Burgess, S. A.; Joslin, E. E.; Gunnoe, T. B.; Cundari, T. R.; Sabat, M.; Myers, W. H. *Chem. Sci.* **2014**, *5*, 4355.
- (24) Bhalla, G.; Bischof, S. M.; Ganesh, S. K.; Liu, X. Y.; Jones, C. J.; Borzenko, A.; Tenn, W. J., III; Ess, D. H.; Hashiguchi, B. G.; Lokare,

- K. S.; Leung, C. H.; Oxgaard, J.; Goddard, W. A., III; Periana, R. A. *Green Chem.* **2011**, *13*, 69.
- (25) Hong, P.; Yamazaki, H. *J. Mol. Catal.* **1984**, *26*, 297.
- (26) Taube, D.; Periana, R.; Matsumoto, T. U.S. Patent 6127590A, 2000.
- (27) Fujiwara, Y.; Moritani, I.; Danno, S.; Asano, R.; Teranishi, S. *J. Am. Chem. Soc.* **1969**, *91*, 7166.
- (28) Yamada, T.; Sakakura, A.; Sakaguchi, S.; Obora, Y.; Ishii, Y. *New J. Chem.* **2008**, *32*, 738.
- (29) Kubota, A.; Emmert, M. H.; Sanford, M. S. *Org. Lett.* **2012**, *14*, 1760.
- (30) Sasaki, K.; Sakakura, T.; Tokunaga, Y.; Wada, K.; Tanaka, M. *Chem. Lett.* **1988**, *17*, 685.
- (31) Vaughan, B. A.; Webster-Gardiner, M. S.; Cundari, T. R.; Gunnoe, T. B. *Science* **2015**, *348*, 421.
- (32) Webster-Gardiner, M. S.; Fu, R.; Fortman, G. C.; Nielsen, R. J.; Gunnoe, T. B.; Goddard III, W. A. *Catal. Sci. Technol.* **2015**, *5*, 96.
- (33) Webb, J. R.; Pierpont, A. W.; Munro-Leighton, C.; Gunnoe, T. B.; Cundari, T. R.; Boyle, P. D. *J. Am. Chem. Soc.* **2010**, *132*, 4520.
- (34) Widegren, J. A.; Finke, R. G. *J. Mol. Catal. A: Chem.* **2003**, *198*, 317.
- (35) Hamlin, J. E.; Hirai, K.; Gibson, V. C.; Maitlis, P. M. *J. Mol. Catal.* **1982**, *15*, 337.
- (36) Gorelsky, S. I.; Lapointe, D.; Fagnou, K. *J. Am. Chem. Soc.* **2008**, *130*, 10848.
- (37) Sperger, T.; Sanhueza, I. A.; Kalvet, I.; Schoenebeck, F. *Chem. Rev.* **2015**, *115*, 9532.
- (38) Balcells, D.; Clot, E.; Eisenstein, O. *Chem. Rev.* **2010**, *110*, 749.
- (39) Ackermann, L. *Acc. Chem. Res.* **2014**, *47*, 281.
- (40) Boutadla, Y.; Davies, D. L.; Macgregor, S. A.; Poblador-Bahamonde, A. I. *Dalton Trans.* **2009**, 5820.
- (41) Webb, J. R.; Burgess, S. A.; Cundari, T. R.; Gunnoe, T. B. *Dalton Trans.* **2013**, *42*, 16646.
- (42) Gunnoe, T. B. *Eur. J. Inorg. Chem.* **2007**, 2007, 1185.
- (43) Shiotsuki, M.; White, P. S.; Brookhart, M.; Templeton, J. L. *J. Am. Chem. Soc.* **2007**, *129*, 4058.
- (44) Oxgaard, J.; Periana, R. A.; Goddard, W. A. *J. Am. Chem. Soc.* **2004**, *126*, 11658.
- (45) Holder, G. A.; Macauley, D. *J. Chem. Eng. Data* **1992**, *37*, 100.
- (46) Baxter, R. D.; Sale, D.; Engle, K. M.; Yu, J.-Q.; Blackmond, D. G. *J. Am. Chem. Soc.* **2012**, *134*, 4600.
- (47) Northcutt, T. O.; Wick, D. D.; Vetter, A. J.; Jones, W. D. *J. Am. Chem. Soc.* **2001**, *123*, 7257.
- (48) Vetter, A. J.; Flaschenriem, C.; Jones, W. D. *J. Am. Chem. Soc.* **2005**, *127*, 12315.
- (49) Zheng, L.; Wang, J. *Chem. - Eur. J.* **2012**, *18*, 9699.
- (50) Cramer, R. *Inorg. Synth.* **1990**, *28*, 86.
- (51) Bianchi, F.; Gallazzi, M. C.; Porri, L.; Diversi, P. *J. Organomet. Chem.* **1980**, *202*, 99.
- (52) Werner, H.; Poelsma, S.; Schneider, M. E.; Windmüller, B.; Barth, D. *Chem. Ber.* **1996**, *129*, 647.
- (53) Khusniyarov, M. M.; Harms, K.; Burghaus, O.; Sundermeyer, J. *Eur. J. Inorg. Chem.* **2006**, 2006, 2985.
- (54) Xie, L.-H.; Suh, M. P. *Chem. - Eur. J.* **2011**, *17*, 13653.
- (55) Frisch, M. J.; Trucks, G. W.; Schlegel, H. B.; Scuseria, G. E.; Robb, M. A.; Cheeseman, J. R.; Scalmani, G.; Barone, V.; Mennucci, B.; Petersson, G. A.; Nakatsuji, H.; Caricato, M.; Li, X.; Hratchian, H. P.; Izmaylov, A. F.; Bloino, J.; Zheng, G.; Sonnenberg, J. L.; Hada, M.; Ehara, M.; Toyota, K.; Fukuda, R.; Hasegawa, J.; Ishida, M.; Nakajima, T.; Honda, Y.; Kitao, O.; Nakai, H.; Vreven, T.; Montgomery, J. A., Jr.; Peralta, J. E.; Ogliaro, F.; Bearpark, M. J.; Heyd, J.; Brothers, E. N.; Kudin, K. N.; Staroverov, V. N.; Kobayashi, R.; Normand, J.; Raghavachari, K.; Rendell, A. P.; Burant, J. C.; Iyengar, S. S.; Tomasi, J.; Cossi, M.; Rega, N.; Millam, N. J.; Klene, M.; Knox, J. E.; Cross, J. B.; Bakken, V.; Adamo, C.; Jaramillo, J.; Gomperts, R.; Stratmann, R. E.; Yazyev, O.; Austin, A. J.; Cammi, R.; Pomelli, C.; Ochterski, J. W.; Martin, R. L.; Morokuma, K.; Zakrzewski, V. G.; Voth, G. A.; Salvador, P.; Dannenberg, J. J.; Dapprich, S.; Daniels, A. D.; Farkas, Ö.; Foresman, J. B.; Ortiz, J. V.; Cioslowski, J.; Fox, D. J. *Gaussian 09*; Gaussian, Inc.: Wallingford, CT, 2009.
- (56) Becke, A. D. *Phys. Rev. A: At., Mol., Opt. Phys.* **1988**, *38*, 3098.
- (57) Lee, C.; Yang, W.; Parr, R. G. *Phys. Rev. B: Condens. Matter Mater. Phys.* **1988**, *37*, 785.
- (58) Grimme, S.; Ehrlich, S.; Goerigk, L. *J. Comput. Chem.* **2011**, *32*, 1456.
- (59) Marenich, A. V.; Cramer, C. J.; Truhlar, D. G. *J. Phys. Chem. B* **2009**, *113*, 6378.
- (60) Zhao, Y.; Truhlar, D. G. *Theor. Chem. Acc.* **2008**, *120*, 215.